Virtual Testing of Composites Using Abaqus

W. Wilson

Fokker Landing Gear B.V., The Netherlands

Abstract: Fokker Landing Gear has a history in the development of composite technology development for landing gear applications. To be able to design and qualify composite landing gear parts it is essential to determine correct and reliable material properties. The material parameters describing the properties are normally determined by test using coupons based on for instance ASTM guidelines. In previous programs it was noticed that some of these tests give unexpected or even incorrect results for the materials (with large tow sizes) used in landing gears.

To resolve this problem Virtual Testing using Abaqus is being used to determine if the standard test methods will result in the intended material parameters. Additionally these virtual tests are used to better evaluate the test results. As a result the test methods can be modified such that the correct properties are measured. Using this approach it can be assured that accurate values for the required material properties are obtained.

In this study Virtual testing was performed using both Abaqus/Standard and Abaqus/Explicit, using a dedicated user-defined material model developed at Fokker Landing Gear. In this material model the composite constituents (fibers and resin) are modelled as separate materials with their own specific material and failure behavior. The crucial interaction between the fibers and resin is accounted for using a new analytical approach. Damage between plies is accounted for using cohesive surfaces.

Using this material model it has been possible to explain the behavior of coupon tests performed in the past which showed unexpected results, and are currently using it to optimize all future coupon test programs.

Keywords: Braids, Composites, Constitutive Model, Damage, Delamination, Fabrics, Failure, GUI, Landing Gear, User-Defined Material

1. Introduction

Fokker Landing Gear has a history in the development of composite technology development for landing gear applications (Figure 1). To be able to design and qualify composite landing gear parts it is essential have accurate computational models to predict both the mechanical and failure behavior of these composite parts. In addition such a computational model should provide insight and understanding of the behavior of the material and component. For this it is essential to have a model that takes into account the microstructure of the composite. Several software package are available on the market to fulfill (at least partly) these requirement. Examples are Genoa, Helius: MCT, and Digimat-FE. In addition these commercial packages several multi-level frameworks are available in literature that includes the coupling between the micro- and macro structure of a composite (e.g. Kouznetsova, 2001; Miehe, 2002). These software packages and numerical frameworks always have one of the following disadvantages: large computation times, material properties have to be redetermined for changes in microstructure, large number of material parameters or act as a black box.

It was therefore decided to write a dedicated material model that fulfills all the requirements but does not have these limitations. In this material model, which is based on a combination of the MCT theory (Key, 2007) and the fiber reinforced model of (Wilson, 2006), fibers and resin are included as separate materials with their own specific material and failure behavior, both with a limited number of required material parameters. The interaction between the fibers and resin is accounted for using a new analytical approach. For large deformations also the reorientation of the fibers due to deformation is accounted for. This material model as been implemented in both Abaqus/Standard and Abaqus/Implicit using the user-subroutines UMAT and VUMAT.

For such a model to be effective it is essential to determine the correct material properties. Material parameters describing the properties are normally determined by test using coupons based on for instance ASTM guidelines. In previous programs it was observed that some of these tests give unexpected or even incorrect results for the material types used in landing gears.

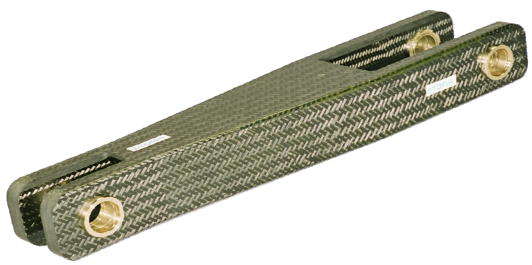

Figure 1. Examples of composite landing gear parts developed by Fokker Landing Gear. Left) Composite drag brace for a large commercial aircraft. Right) Composite trailing arm for the NH90 Helicopter.

The goal of this study is to show the power of Virtual Testing by evaluating and explaining unexpected test results from previous coupon test programs.

2. Methods

2.1 Material model

2.1.1 Total stress

The total stress in the material is given by

$$\boldsymbol{\sigma}_{tot} = \left(1 - \sum_{i=1}^{totf} \rho_f^i\right)\boldsymbol{\sigma}_r + \sum_{i=1}^{totf} \rho_f^i \boldsymbol{\sigma}_f^i \,, \quad \text{Equation 1}$$

where $\boldsymbol{\sigma}_r$ and $\boldsymbol{\sigma}_f$ are the total resin and fiber stress tensors, respectively, and ρ_f^i and σ_f^i are the volume fraction and fiber stress in the *i*-th direction $\vec{e}_f^{\,i}$, respectively. When the strains in a composite are relatively low, it can be assumed that the relative volume fractions of the resin and fiber stay constant during deformation. Hence, ρ_f^i is taken as a constant. Before occurring of damage in the material both the resin and fiber are assumed to behave linear elastic.

2.1.2 Microstructure model

A fiber-reinforced composite consists of fibers embedded in a resin. When loaded all loads are distributed between the fibers and resin. This means that the total amount of stress in the composite is equal to the sum of all stresses in the resin and fibers. The same hold for strains.

The distribution of the total strain over the fibers and resin depends on the stiffness of the two components, their relative volume fractions and the microstructure of the composite. If we for instance look at a composite of which the resin stiffness is much lower than the fiber stiffness, the resin strain in the direction perpendicular to the fiber-direction will be much larger than the fiber strain.

In the material model this distribution of stresses and strains between the resin and fibers is included using an analytical representation of the microstructure. This done by writing the fiber stress tensor $\boldsymbol{\sigma}_f$ as a function of the resin stress tensor $\boldsymbol{\sigma}_r$. The equations to couple the fiber and resin stress tensor are proprietary to Fokker Landing Gear.

2.1.3 Fiber directions and properties

Fiber directions are included as vectors $\vec{e}_f^{\,i}$. The current fiber direction can be written as a function of the deformation gradient tensor (**F**) and the initial fiber direction ($\vec{e}_{f,0}^{\,i}$) as

$$\vec{e}_f^{\,i} = \frac{\mathbf{F} \cdot \vec{e}_{f,0}^{\,i}}{\left\| \mathbf{F} \cdot \vec{e}_{f,0}^{\,i} \right\|}. \quad \text{Equation 2}$$

The logarithmic fiber strains in fiber direction can be computed as

$$\varepsilon_f^i = \vec{e}_f^{\,i} \cdot \boldsymbol{\varepsilon}_{\text{tot}} \cdot \vec{e}_f^{\,i}, \text{ Equation 3}$$

where $\boldsymbol{\varepsilon}_{\text{tot}}$ is the strain tensor of the composite.

As mentioned above, the fibers are assumed to behave linear elastic. However, the fibers are assumed to have a different stiffness in compression and tension, as

$$\begin{array}{lll} E_f = E_{ft} & \text{for} & \varepsilon_f \geq 0 \\ E_f = E_{fc} & \text{for} & \varepsilon_f < 0 \end{array}. \quad \text{Equation 4}$$

2.1.4 Failure behavior

Fiber damage is assumed to be a brittle fracture. Although it is assumed that a fiber fails immediately once damaged, the total damage in a fiber bundle is assumed to evolve more gradually, this mainly due to the differences in fiber orientations and resin distribution around the fibers (which influences the local fiber stresses). The following function for the evolution of the damage parameter D is used

$$D_f = \left(\frac{\kappa_c}{\kappa}\right)\left(\frac{\kappa - \kappa_i}{\kappa_{c,f} - \kappa_i}\right)$$. Equation 5

Here the history parameter κ is the maximum value of the absolute fiber strain over time, and κ_i and κ_c are the values at which damage initiation starts and at which the fibers have completely failed.

Resin damage will in most cases start around the fibers at locations where there are high strain concentrations. As the local strains concentration can be much larger than the average resin strain this initial damage can start at relatively low average resin strains. As this initial damage is very local it is assumed to hardly affect the overall stiffness. Due to this the damage evolution speeds will be very low just after damage initiation. Only when the amount of damage becomes significant the speed of damage evolution will increase rapidly. This means that the process of damage progression takes place relatively slow, and that there is a large difference between the composite strain at which resin damage is initiated and the strain at which it completely fails. The equation to model damage progression is proprietary to Fokker Landing Gear.

When the resin is damaged it is assumed to slowly crumble. This means that when fully damaged the material can still carry compressive loads (crumbles are being compressed together), but can no longer carry any tensile or shear loads. To include this, the 4th order resin stiffness matrix is written as

$$^4\mathbf{C}_r = \begin{cases} K\mathbf{II} + 2(1-D)G\left({}^4\mathbf{I} - \frac{1}{3}\mathbf{II}\right) & \text{for} \quad \varepsilon_{r,vol} \le 0 \\ (1-D)K\mathbf{II} + 2(1-D)G\left({}^4\mathbf{I} - \frac{1}{3}\mathbf{II}\right) & \text{for} \quad \varepsilon_{r,vol} > 0 \end{cases}$$, Equation 6

where $\mathbf{I}$ and $^4\mathbf{I}$ are the second and fourth-order unit tensors, respectively, and K and G and the bulk and shear modulus, respectively.

2.1.5 Implementation in Abaqus

The material model as discussed in the previous chapter has been implemented in the finite element package Abaqus for:

- Abaqus/Explicit: large deformations and solid elements
- Abaqus/Explicit: large deformations and shell elements
- Abaqus/Standard: large deformations and solid elements
- Abaqus/Standard: large deformations and shell elements
- Abaqus/Standard: small deformations and solid elements
- Abaqus/Standard: small deformations and shell elements

In Abaqus/Explicit this is done using the user-subroutine VUMAT and in Abaqus/Standard using the user-subroutine UMAT.

A special GUI for Abaqus/CAE has been developed for modeling large tow size fabrics and braids have been developed using the RSG Dialog Builder in Abaqus/CAE. As an example the GUI for modeling a fabric is given (Figure 3).

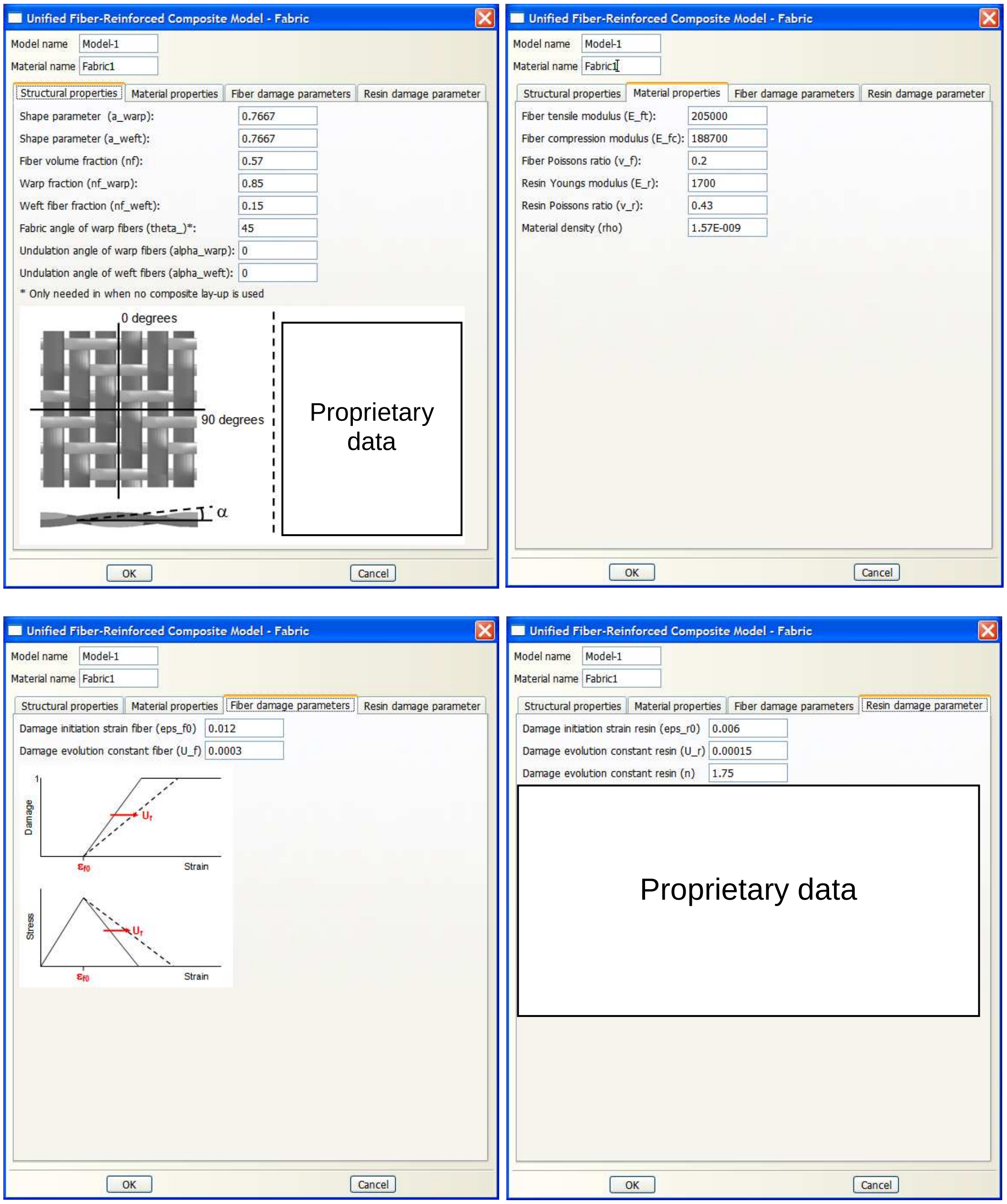

Figure 3. GUI in Abaqus/CAE for creating a fabric material model

2.2 Determination of material parameters

For the examples shown in this article test data from a 2x2 twill fabric and several braids, both with the same carbon fibers and epoxy resin are used. The unknown material parameters of these composites are determined by fitting FEA models to experimental coupon test data.

2.2.1 Fitting procedure

The fitting procedure is performed iteratively, using a multidimensional unconstrained non-linear minimization procedure available in Matlab 7.0 called "fminsearch". From within this procedure ABAQUS is called to run the FEA models. The results of the simulations are then transferred back to Matlab, where they are compared with the experimental data. During the first iteration all test are simulated using an initial set of material parameters. During the subsequent iterations the material parameters will be adjusted by Matlab to minimize the error between the experimental and FEA results. The end result will be a set of material data for which the numerical model describes all experiments best. To be sure that a unique set of material parameters is obtained, the fit is started several times with a different set of initial parameter values.

The following objective function is minimized:

$$f = \sum_{j=1}^{N=9} \frac{w_j}{M_j} \sum_{i=1}^{M_j} \frac{\left(\varepsilon_{\exp,j}(i) - \varepsilon_{FEA,j}(i)\right)^2}{\varepsilon_{\exp,j}(i)}, \qquad \text{Equation 7}$$

where N is the number of experimental data curves, and M_j and w_j are the number of data points and the weighting factor for curve j, and ε_{exp} and ε_{FEA} are the measured and computed strains, respectively.

2.2.2 Results

First al unknown material properties were fitted on coupon test data from the fabric.
These unknown material parameters are:

E_m	Young's modulus of the resin
E_{fc}	Young's modulus of the fibers in tension
E_{ft},	Young's modulus of the fibers in compression
υ_f	Poisson's ratio of the fibers
υ_m	Poisson's ratio of the resin
ε_0	Resin damage parameter
C_r	Resin damage parameter
n	Resin damage parameter
a_{warp}	Shape parameter that defines the microstructure
a_{weft}	Shape parameter that defines the microstructure

After this fit all structure independent material parameters (E_m, E_{fc} E_{ft}, υ_f, υ_m) were held constant, and the remainder of the parameters (ε_0, C_r and n and a_{braid}) were fitted on coupon test data from the braids. The resulting fits are plotted in Figure 4 and 5. Note that fiber failure was not accounted for in this example, hence fibers strains stayed below their failure strains.

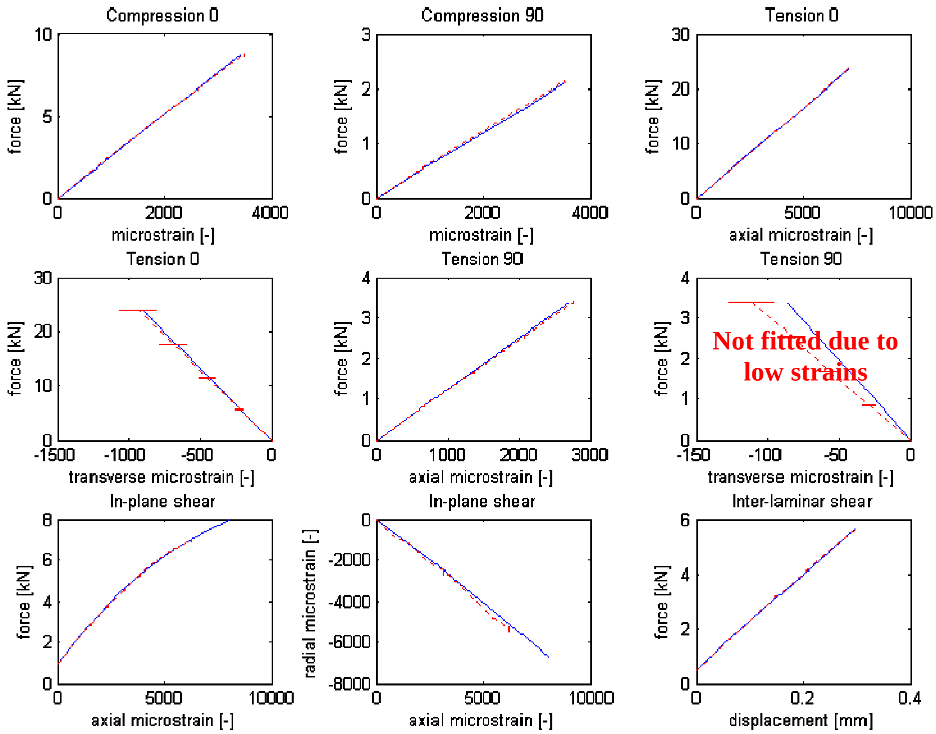

Figure 4. Results parameter fit for twill fabric

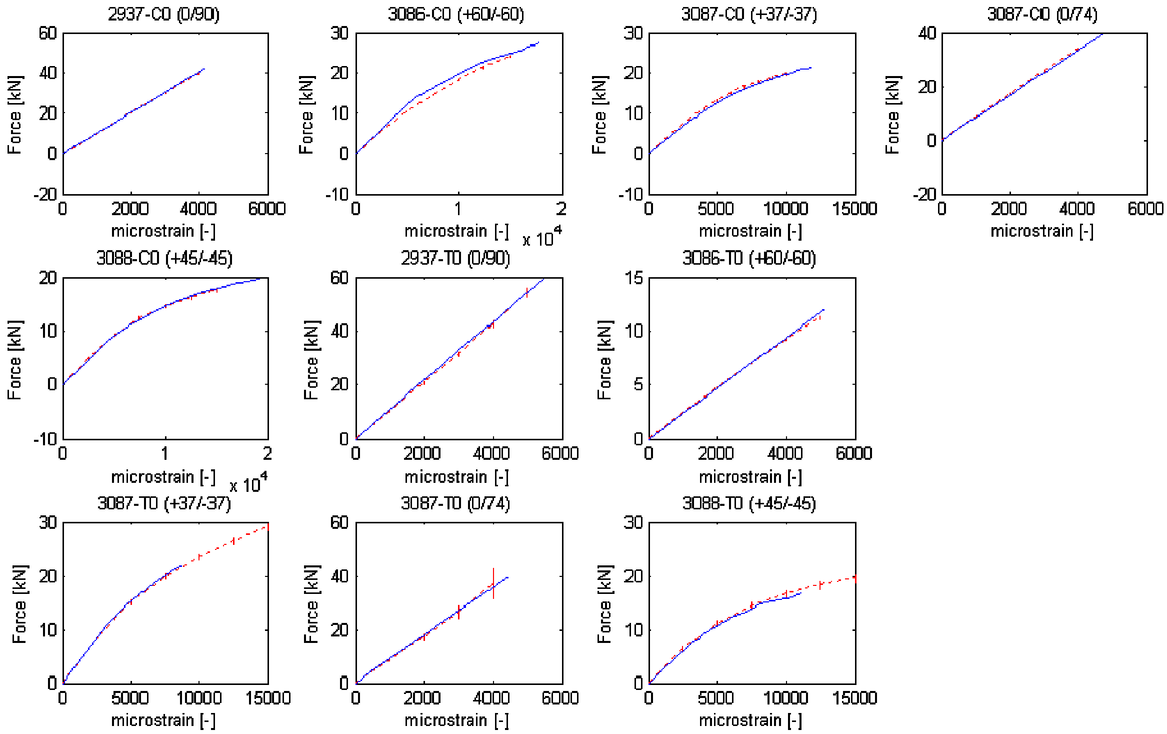

Figure 5. Results parameter fit for braids (the values between brackets are the directions of two fiber bundles)

3. Virtual testing examples

3.1 Uni-axial tension of a fabric

During the coupon testing program a tensile test was performed according to ASTM D3039-00. An example of a resulting failed coupon is shown in Figure 6. All coupons showed a fracture at 3 locations, while one single fracture was expected. Also delamination at the edges of the fracture at the center were found, while these are normally only found after compressive failures.

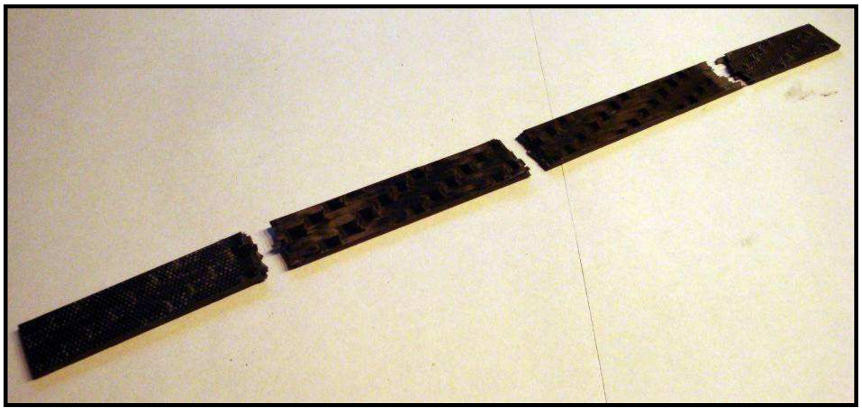

Figure 6. Failuled tensile test coupon.

To explain these results a virtual coupon test was performed using Abaqus/Explicit. The material model as discussed in the previous chapter was used as the material model. Each ply was modeled as a separate element layer. The layers were tied together using cohesive surfaces. Damage initiation and growth behavior was including in the material description of the cohesive surfaces to model possible delaminations. The “general contact” algorithm was used to model possible contact between all elements. To model consisted of 1700 elements of type C3D8R with enhanced hourglass control. Boundary conditions were chosen such that the mimic the test conditions most accurately. Total run-time on 1 CPU of an Intel Xeon 6160 (3GHz) was approximately 8 hours.

In Figure 7 the deformed model is shown at different time increments. The model showed the following:

1. The sample breaks in the center due to excessive tensile strains (1st failure location) (Figure 7a)
2. Due to the high amount of energy released in the fracture, the two halves snap back and move towards the clamps at the edges (Figure 7b).
3. The shockwave hits the clamps resulting in compressive failure (2nd and 3rd failure location) (Figure 7c)
4. Again, the now 2 loose parts, snap back and hit each other in the center, resulting in delaminations at the initial failure site in the center (Figure 7D)

Hence, the virtual test gave an unexpected but very plausible explanation for the observed failure in the real test.

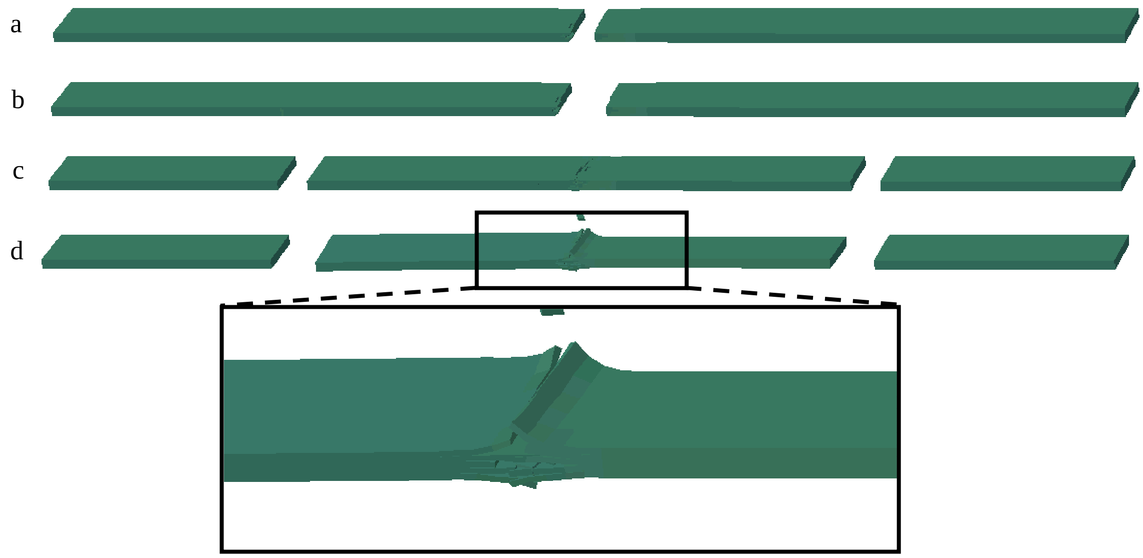

Figure 7. Deformed tensile test model at different time increments

3.2 Uni-axial compression of a fabric

During the coupon tests on the fabric it was found that the compressive strength in warp direction was only half of the tensile strength. This compressive strength was much lower than expected.

Virtual testing using Abaqus/Explicit was used to for an explanation for this low compressive strength. The material model as discussed in the previous chapter was used and again each ply was modeled as a separate element layer. The layers were tied together using cohesive surfaces. Damage initiation and growth behavior was including in the material description of the cohesive surfaces to model possible delaminations. The “general contact” algorithm was used to model possible contact between all elements. The model consisted of 650 elements of type C3D8R with enhanced hourglass control. Boundary conditions were chosen such that the mimic the test conditions most accurately. Total run-time on 1 CPU of an Intel Xeon 6160 (3GHz) was approximately 3 hours.

In Figure 8 the deformed model, with contour plots of the damage in the cohesive surfaces, is shown at different time increments. As can be seen in Figure 8 after a certain amount of compression the sample slowly started to buckle. With increasing amount of buckling delaminations between the different plies is initiated, resulting in failure of the sample. The failure load that was determined using the virtual test was only 3 percent lower than the failure force measured in the real test, showing the accuracy of the model

Hence, the virtual test gave a plausible explanation for the observed compressive strength.

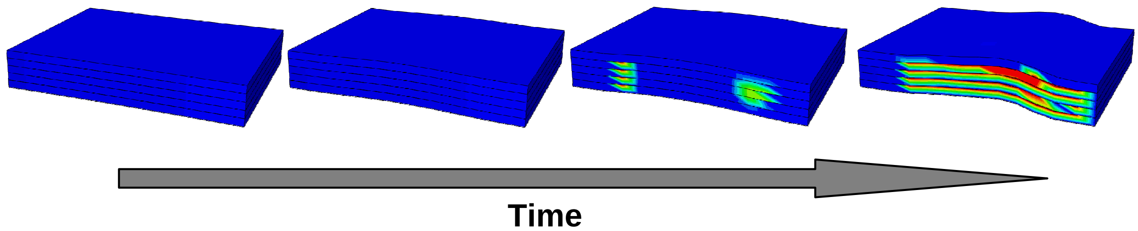

Figure 8. Deformed compression test model at different time increments, with contourplots of the amount of damage in the cohesive surfaces (blue= no damage, red= complete failure)

3.3 Uni-axial tension/compression of braid

From the coupons on the braids it was found that the compressive and tensile stiffness and strength of a 45-degrees braid (Figure 9) were different. As these properties are mainly determined by the resin properties this was unexpected.

To explain these differences Virtual coupons tests were performed using Abaqus/Standard. The material model as discussed in the previous chapter was used as the material model. The part representing the composite coupon was meshed such that each ply was modeled as a separate element layer. The model for the compression case consisted 344 of elements were type C3D8, and the model for the tensile case consisted 1277 of elements were type C3D8. Boundary conditions were chosen such that the mimic the test conditions most accurately. Total run-time on 1 CPU of an Intel Xeon 6160 (3GHz) was in the order of minutes.

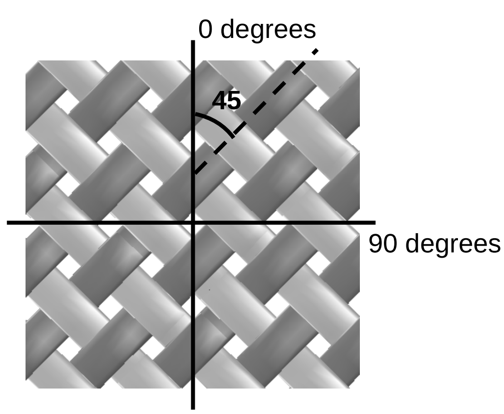

Figure 9. Schematic of 45-degrees braid.

In Figure 10 a contour plot shows the absolute strain in the longitudinal direction, of the free sections of the compression and tensile test are given. As can be seen the compression test samples were much shorter than the tensile test samples, this to prevent buckling in the compression test. The squares in the center of the samples show the location of the strain gauges that were used in the actual test.

From both models it followed that the maximum strains were location at approximately an angle of 45 degrees from the corners of the free section. In case of the compression test the location of the two strain peaks coincide, leading to larger strains. This might explain the found difference in compressive and tensile strength.

As can be seen in Figure 10 in the compression test the strain gauge was located at the site of the strain peak, which was not the case for the tensile test. Hence, when the samples would be strained with the same global absolute strain, the local strain in the compression test will be higher. This can explain the difference in the found compression and tensile stiffness.

Hence, again the virtual tests could explain the unexpected test results.

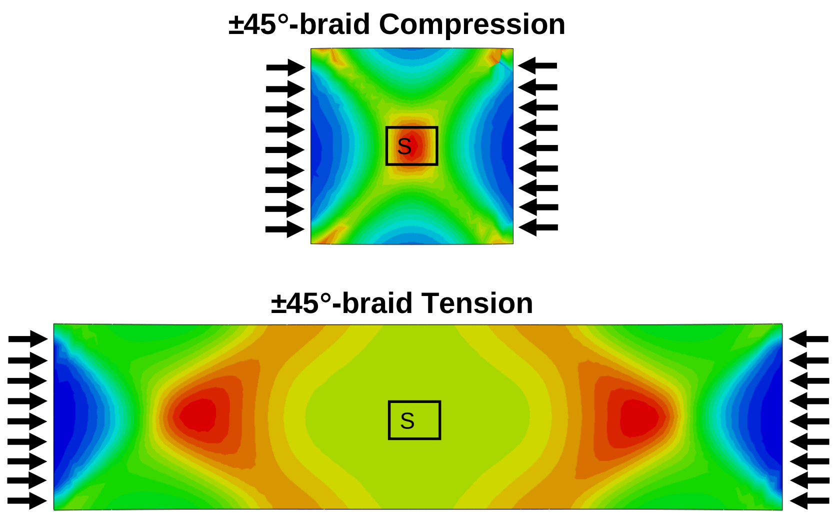

Figure 10. Contourplot showing the absolute maximum strains in longitudinal direction for the 45 degrees braid compression (top) and tensile (bottom) test. The squared with an S show the location of the strain gauges in the real test.

4. Discussion

In this study virtual testing was used to explain unexpected rest results from coupon test. For this a user-defined material model was used, that has been developed by Fokker Landing Gear. It is shown that with this material model both fabric and braid test data can be described with the same set of material parameters. Only 4 structure dependent parameters had to be determined separately for twill fabric and braid. This indicates that the "Unified Fiber-Reinforced Composite"-model is indeed capable of describing composites with any type of fiber structure.

In the virtual test examples shown in the article, virtual testing has been successfully used to explain unexpected coupon test results. By performing virtual tests, much more insight was gained in the material behavior of the used composites.

Of course it is prefered to perform virtual testing (with estimated material properties) prior to performing the actual test. Virtual testing can then be used to optimize test methods prior to testing. This way it can be ensured, that all tests provide the most accurate results.

Apart from using virtual testing for optimizing coupon tests or explaining their results, it can of course be used to optimize any type of test.

Especially for test performed on simplified geometries or subcomponents it can be difficult to determine the correct boundary conditions to be used in the test. For instance, instead of determining the amount of damage locally by testing a full brace, it is much simpler to do it on just a part of the brace. However, this will only give representative results if the used boundary conditions mimic the real loading conditions. In such a case virtual testing can be used to optimize these boundary conditions such that the resulting damage is the same as for an impact on a full brace.

To conclude, virtual testing can be a very useful tool to optimize tests and to explain their results, resulting in better tests and more insight in the behavior of the tested materials or parts.

5. References

1. Crisfield, M. A, “Variable Step-Length for Nonlinear Structural Analysis,” Report 1049, Transport and Road Research Lab., Crowthorne, England, 1982.
2. Key, C. T., Schumacher S, C., and Hansen, A. C. “Progressive failure modeling of woven fabric composite materials using multicontinuum theory”, Composites Part B: Engineering, 38(2):247-257, 2007
3. Kouznetsova, V., Brekelmens, W., and Baaijens, F. “An approach to micro–macro modeling of heterogeneous materials”. Computational Mechanics, 27:37–48, 2001.
4. Miehe, C., Schroder, J., and Becker, M. “Computational homogenization analysis in finite elasticity: material and structural instabilities on the micro– and macro–scales of periodic composites and their interaction”. Computer Methods in Applied Mechanics and Engineering, 191:4971–5005, 2002.
5. Wilson W, Huyghe, J., M,, R, J., van Donkelaar, C., C. “A composition-based cartilage model for the assessment of compositional changes during cartilage damage and adaptation”, Osteoarthitis and Cartilage, 14(6):507–616 2006